Ravi Subrahmanyan
CSIRO-S&A, Curtin-CIRA
March 2022

Stokes imaging/beamforming with SKA Low Station AAVS2

Summary

This note reports on polarisation calibration and imaging of intra-station correlations in SKA LOW station prototype AAVS2, aimed at evaluating polarisation purity in station beamforming. The dataset analysed was a 24-hr observing session in a single coarse frequency channel 1-MHz wide at 110 MHz.

AAVS2 intra-station XX and YY correlations were modelled using embedded element patterns (EEPs) and a Global sky model + Sun, assuming the sky brightness to be unpolarised. Antenna-based complex gains versus time for X and Y polarisation receiver chains were solved for by comparing model with measured visibilities in XX and YY products, respectively. These X and Y complex gain solutions were used to calibrate the XX, XY, YX and YY visibility correlations.

Following this, XY phase offset was solved for by comparing these gain-calibrated measured visibilities in XY and YX correlations with model visibilities; model predictions were based on the unpolarised sky model. The derived XY phase was stable over the 24 hr observing and XY and YX visibility measurements at all times were corrected for this XY phase offset.

Python 3 scripts were written to combine the four correlation products and compute healpix sky images in Stokes parameters, while also correcting for embedded antenna-based voltage beam patterns that encode the direction-dependent responses of the polarised feeds.

- As a result of the accuracy of the calibration and of the beam patterns, leakage of Stokes I into Stokes Q and U within any station beam is less than 3% and into Stokes V is less than 1%, for elevations above 45 degrees.

- Limitations in the accuracy of the beam models results in that Stokes I flux density leaks into Stokes Q, U and V across the whole visible sky. Every Stokes I pixel leaks with standard deviation 0.15% into Stokes Q & U over the whole field of view, and into Stokes V with standard deviation 0.05%.

- The consequent limit on polarisation purity in station beams in Stokes parameters will naturally then depend on the brightness distribution in the sky at that time. When the Galactic centre is close to zenith at MRO and the brightest parts of the Galactic plane are above horizon, Stokes images have standard deviations of 370 K in Q & U and 55 K in Stokes V. These are less than 1% of the Stokes I peak of 44,670 K towards the Galactic Centre; however, they are a substantial fraction of the mean brightness temperature of the sky at this frequency.

The dominant limiting factor for polarisation purity in beams of SKA station AAVS2 is the accuracy of the average antenna voltage patterns — common-mode error across the EEPs of the station — causing leakage from Stokes I into Q, U and V at the source pixel and also across the entire sky. A possible approach to overcome this limitation might be to include a direction dependent Jones matrix in the calibration solution, to represent common-mode correction to the EEPs.

Measurement set

The data are from an acquisition made during 21/22 April 2020 with the AAVS2 station, which consists of a 2D pseudo-random configuration of 256 SKALA4.1 antennas over a 38-m diameter ground area. Intra-station visibilities were recorded in a pair of adjacent 0.14-sec integrations and these pairs of snapshot observations were repeated every 5 mins over about 24 hours. The observations commenced in the evening of 21st April at about 1830 hrs local AWST time and ended 24 hrs later in the evening of 22nd April. The antenna signals were sampled at 800~MHz and channelised to give 512 coarse channels over 400 MHz. Digital data in a single coarse channel number 141, which has a noise equivalent width of 0.926 MHz centred at 110 MHz, was finely channelised over 32 frequency channels. Intra-station correlations were computed and recorded in these 32 fine frequency channels with 0.14-sec integration time.

At each integration time, all 32 channel data corresponding to each visibility correlation product were averaged together in frequency. Visibility pairs, with 0.14-sec integration and at adjacent times, were averaged together. Examination of the visibilities indicated that six of the 256 antennas were faulty and the data products involving those antennas were rejected. Thus the visibility data used in the analysis reported here consists of snapshot continuum visibility measurements, in XX, XY, YX and YY polarisations, in each of $250 \times (250 - 1)/2 = 31125$ baselines, spaced 5 minutes apart. The measurement data used here are initially "uncalibrated" in the sense that no prior bandpass or complex gain calibrations were applied to the intra-station correlations.

It may be noted here that X-polarisation in the SKALA4.1 antennas of the station are oriented EW and Y-polarisation is NS.

Polarisation Calibration

The GDSM global sky model [Zheng et al. 2016] implemented in PyGSM was used to represent the sky as a healpix image. The Sun was added in at each timestamp assuming the flux density model in Benz [2009 Astronomy & Astrophysics, Vol. 4B, p.103] and computing its ephemeris sky position. The Sun was added in a pixel as a uniform brightness temperature of value corresponding to the flux density and resolution of the healpix representation. The sky model was unpolarised.

The beam models are from the EM simulation groups at Curtin-CIRA and INAF, using FEKO, which provide complex voltage patterns over sky azimuth-elevation, separately for each of X and Y feeds of each of the 256 embedded SKALA4.1 antennas in the AAVS2 station. The patterns of each of X and Y feeds in any antenna provides the complex voltage gain to vertical and horizontal sky polarisation. In principle, I expect that once the embedded element patterns (EEPs) are used in the measurement equation, and if they are accurate, there ought to be no residual "leakage terms" assuming that the electronics receiver chains are well isolated.

The visibility modelling is described in a Memo available at https://www.atnf.csiro.au/observers/memos/Modelling_Calibration_Imaging_intrastation_correlations_in_AAVS2_at_110_MHz.pdf in which Stokes I imaging was described. In brief, the model visibilities are computed, using a custom Python 3 script, for each AAVS2 baseline, at each timestamp corresponding to the measurement data, in XX and YY correlations, and taking into account the embedded element patterns (EEPs) for all antennas in the station. The Fourier transform was from curved healpix celestial sphere to 3D u, v, w visibility space.

MIRIAD task SELFCAL was used to solve for antenna based complex gains separately at each timestamp and in X and Y receiver chains. The model XX correlations were compared with measurement XX correlation to derive X gains, and similarly for Y gains.

The gain tables computed by MIRIAD SELFCAL provide complex gain values that measurements are to be multiplied by to get calibrated visibilities. All the four polarisation products — XX, XY, YX, YY — corresponding to each baseline and timestamp of the measurement data were calibrated using appropriate pairs of the X and Y receiver gains and using conjugates of the gains for the second antenna in the pair. No smoothing or interpolations of gain solutions were performed: gains computed independently at each timestamp were applied to correlations at that timestamp.

Calibrating for XY phase

Calibrating XY phase in stations is important since the XY and YX complex products contribute to all Stokes parameters, including Stokes I, at sky positions off zenith and away from azimuth 0, 90, 180 and 270 deg.

At the time when the Galactic Centre was close to zenith, the unpolarised Stokes I sky model was used to predict all four visibility products — XX, XY, YX and YY — on all baselines. Fig. 1 below shows scatter plots comparing model predictions and calibrated measurements of visibility amplitudes.

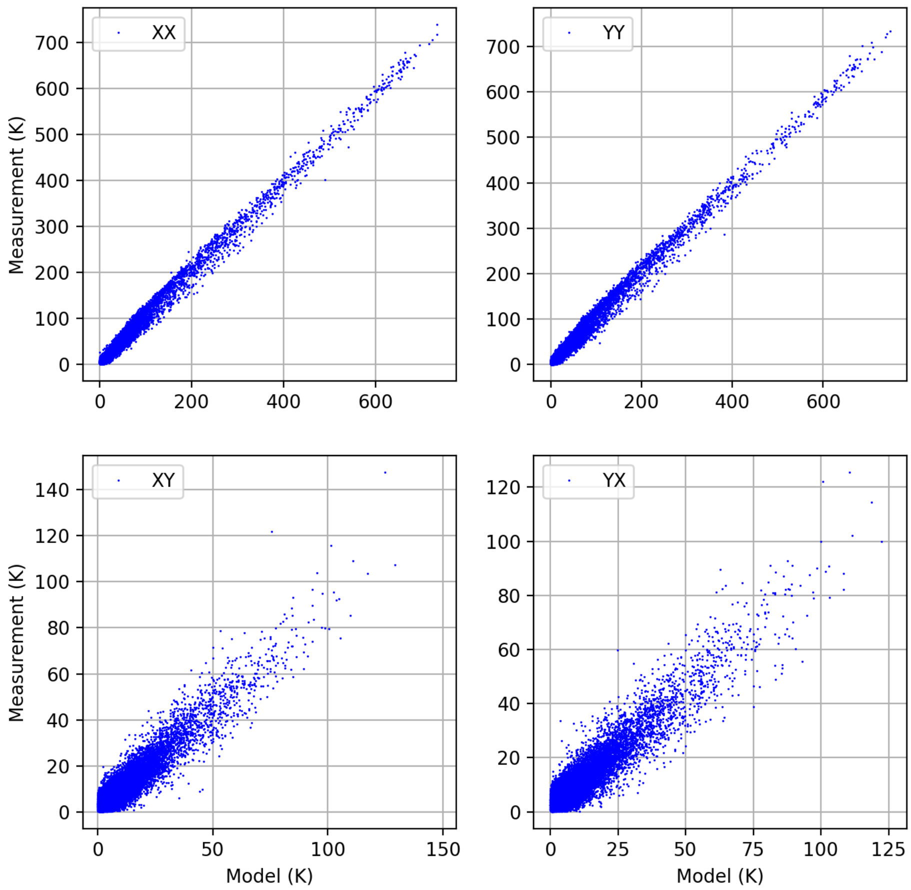

Fig 1: Scatter plot comparing amplitudes of visibilities: model predictions versus calibrated measurements. The visibilities are from a single snapshot when the Galactic Centre was close to zenith.

Scatter plots for XY phase are shown in Fig. 2. As expected, the model predictions and calibrated measurements match for XX and YY products, since the measurements have been corrected for X and Y channel complex gains. However, the XY and YX products display an offset — common for all baselines — because of the as yet uncalibrated phase difference between the X and Y receiver chains.

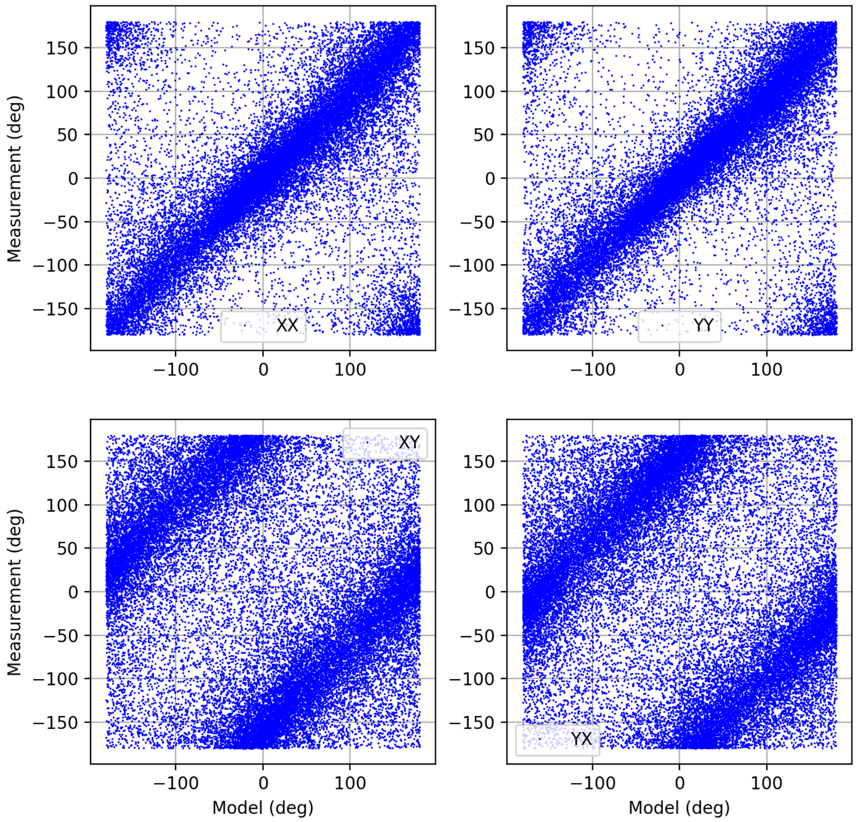

Fig 2: Scatter plot comparing phases of visibilities, model predictions versus calibrated measurements. The visibilities are from a single snapshot when the Galactic Centre was close to zenith.

The XY and YX phase scatter was used to solve for a common phase offset, the fit yielded 158.5 degrees from the XY scatter and -159.7 degrees from the YX scatter.

Since the complex gains of X and Y receiver channels have been independently solved and corrected for, drift in XY phase of the reference antenna over time will appear as a drift in the above-measured common phase offset. I have computed the common phase offset between model predictions and calibrated measurements at a few times, using snapshot visibilities; the values are listed in the table below:

UT	Remark	XY	YX	Mean XY phase
20h	Galactic Centre close to zenith	158.5	-159.7	159.1
4h	Sun at meridian crossing	160.4	-158.1	159.3
6h	Sun at Az = -38 deg, El = 42 deg	158.4	-158.0	158.2
10h	Sun and Galaxy below horizon	162.0	-160.8	161.4

The XY phase appears stable, at least for the reference antenna. The XY phase appears to be reliably derivable from snapshot data, over varied conditions of celestial emission. A value of 159.5 degrees is adopted as the XY phase for AAVS2 at 110 MHz, for this dataset. The XY phase offset is applied as an additional calibration at all times for the XY and YX products.

Stokes Imaging using embedded beam patterns

I have chosen to represent the sky as an all-sky healpix grid: a grid of pixel locations with fixed celestial coordinates on the celestial sphere. The imaging of polarisation products to Stokes sky pixels is performed as a two step process. First, at each time, 4-vectors $[R_{XX}, R_{XY}, R_{YX}, R_{YY}]^T$ that represent visibility coherency in different baselines are transformed to direction-dependent Stokes visibility vectors $[I_v, Q_v, U_v, V_v]^T$. Next, the Stokes visibilities are 3D Fourier transformed from u, v, w spatial frequency or visibility domain to the celestial sphere, to get Stokes intensities $[I, Q, U, V]^T$ at every healpix pixel. The first step accounts for the direction dependent gains of the embedded antennas; the second step accounts for the geometric delays. The polarisation imaging at each timestamp provides Stokes images at all sky pixels above horizon at that instant, corrected for the dissimilar EEP beams.

The linear dipole-like feeds of the SKALA4.1 antennas are connected to their respective receiver chains with a polarity that corresponds to the X-polarisation directed towards East and Y-polarisation towards North. The polarity is determined by which arm of the dipole connects to the signal terminal of the amplifier and which arm connects to ground: the eastern and northern arms of the dipoles are connected to amplifier input terminals and the western and southern arms are connected to amplifier grounds. The measured coherency vector $[R_{XX}, R_{XY}, R_{YX}, R_{YY}]^T$ corresponding to any baseline is determined by the E-field $[E_{1X}, E_{1Y}]^T$ at the terminals of one antenna along with the corresponding E-field $[E_{2X}, E_{2Y}]^T$ at the terminals of the second antenna. This measured coherency vector is the Kronecker product

$$\begin{bmatrix} R_{XX} \\ R_{XY} \\ R_{YX} \\ R_{YY} \end{bmatrix} = \begin{bmatrix} E_{1X} \\ E_{1Y} \end{bmatrix} \otimes \begin{bmatrix} E^*_{2X} \\ E^*_{2Y} \end{bmatrix}.$$

The FEKO EM modelling provides beam patterns using spherical convention with the horizontal component moving anti-clockwise from East to North and vertical component in the same convention as Zenith angle. I have transformed the frame of the complex patterns to horizontal H and vertical V polarisation components in every sky direction, assuming a convention that has the sky horizontal component H directed towards increasing Azimuth and vertical V component directed towards increasing Elevation. It may be noted here that Azimuth increases from North towards East.

The complex gains of any antenna towards a sky direction thus defines a Jones matrix, which transforms the $[E_H, E_V]$ field incident from that sky direction to $[E_X, E_Y]$ voltages at the antenna terminals:

$$\begin{bmatrix} E_X \\ E_Y \end{bmatrix} = \begin{bmatrix} B_{X\phi} B_{X\theta} \\ B_{Y\phi} B_{Y\theta} \end{bmatrix} \begin{bmatrix} E_H \\ E_V \end{bmatrix}.$$

Here $B_{X\phi}$ and $B_{X\theta}$ represent the complex beam response of the X polarisation feed of the antenna to horizontal and vertical polarisation components, respectively, of the incident field. Similarly, $B_{Y\phi}$ and $B_{Y\theta}$ represent complex beam response of Y polarisation of the antenna to horizontal and vertical polarisation components, respectively, of the incident field. These are the beam patterns computed in EM simulations and whether they are used directly or their complex conjugates are used depends on the sign of the exponent in the Fourier transform from visibility domain to celestial sphere, which is simply decided by convention. I have found that for the convention adopted in acquisition of the measurement data in AAVS2, complex conjugates of the FEKO model beam patterns are to be used for transforming fields from celestial sphere to visibility domain.

The average complex antenna patterns are shown in Figs. 3 & 4 in the following page: amplitudes and phases are shown separately. These are averages over the 256 embedded element patterns and not the patterns for an isolated antenna. The amplitude and phase patterns for one of the embedded antennas — antenna number 105 — is shown in Figs. 5 & 6 as examples of EEPs.

In any sky direction, the incident E-fields $[E_{1H}, E_{2V}]$ and $[E_{2H}, E_{2V}]$ determine the coherency vector $[R_{HH}, R_{HV}, R_{VH}, R_{VV}]$ in the *H-V* frame tangent to the celestial sphere. The coherency vector is, once again, a Kronecker product:

$$\begin{bmatrix} R_{HH} \\ R_{HV} \\ R_{VH} \\ R_{VV} \end{bmatrix} = \begin{bmatrix} E_{1H} \\ E_{1V} \end{bmatrix} \otimes \begin{bmatrix} E^*_{2H} \\ E^*_{2V} \end{bmatrix}.$$

In any baseline, the coherency vector that is described in the *H-V* frame towards a sky direction may be transformed to a coherency vector that is described in the *X-Y* reference frame at the antenna terminals. The 4×4 matrix that describes this transformation is the Kronecker product of the Jones matrices describing the complex antenna beam patterns:

$$\begin{bmatrix} R_{XX} \\ R_{XY} \\ R_{YX} \\ R_{YY} \end{bmatrix} = \left(\begin{bmatrix} B_{1X\phi} B_{1X\theta} \\ B_{1Y\phi} B_{1Y\theta} \end{bmatrix} \otimes \begin{bmatrix} B^*_{2X\phi} B^*_{2X\theta} \\ B^*_{2Y\phi} B^*_{2Y\theta} \end{bmatrix} \right) \begin{bmatrix} R_{HH} \\ R_{HV} \\ R_{VH} \\ R_{VV} \end{bmatrix}.$$

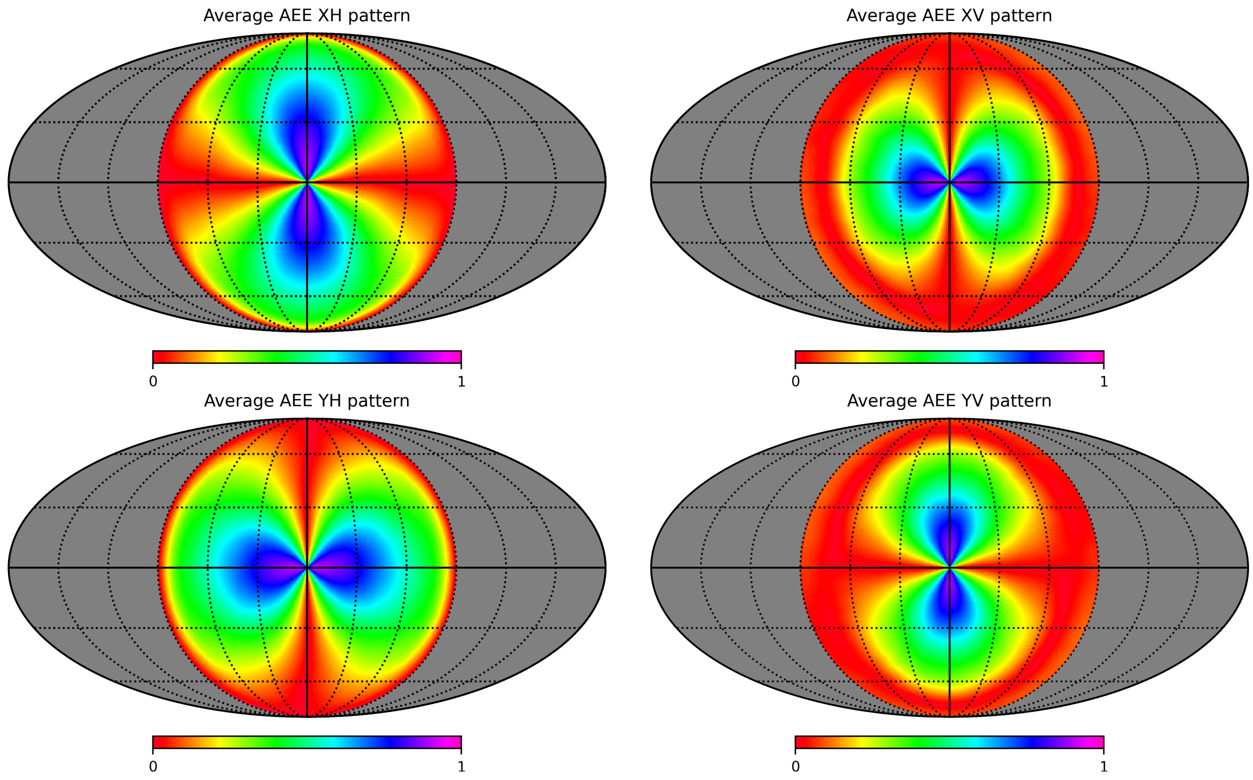

Figure 3 above shows the amplitudes of the average embedded element patterns. The images are in sky projection with North upwards, East to the left and zenith at the centre.

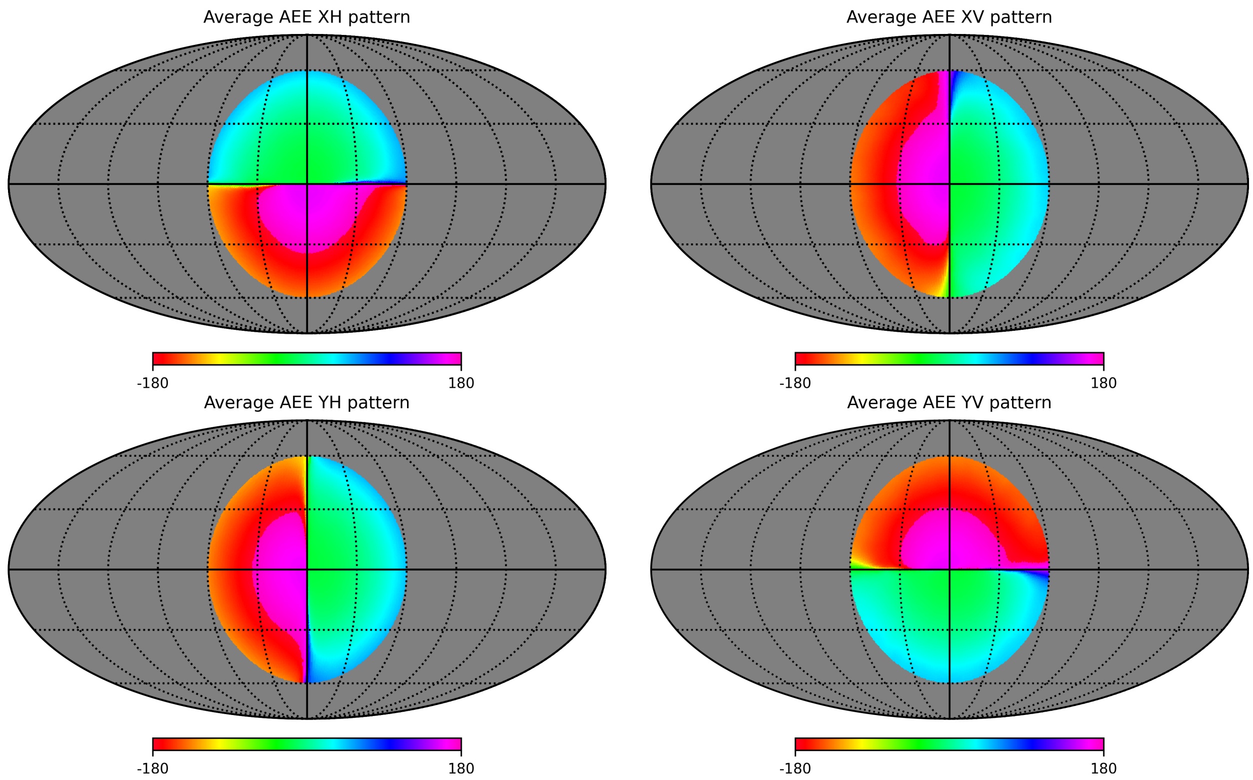

Figure 4 above shows the phase of the average embedded element patterns, limited to elevations above 30 degrees.

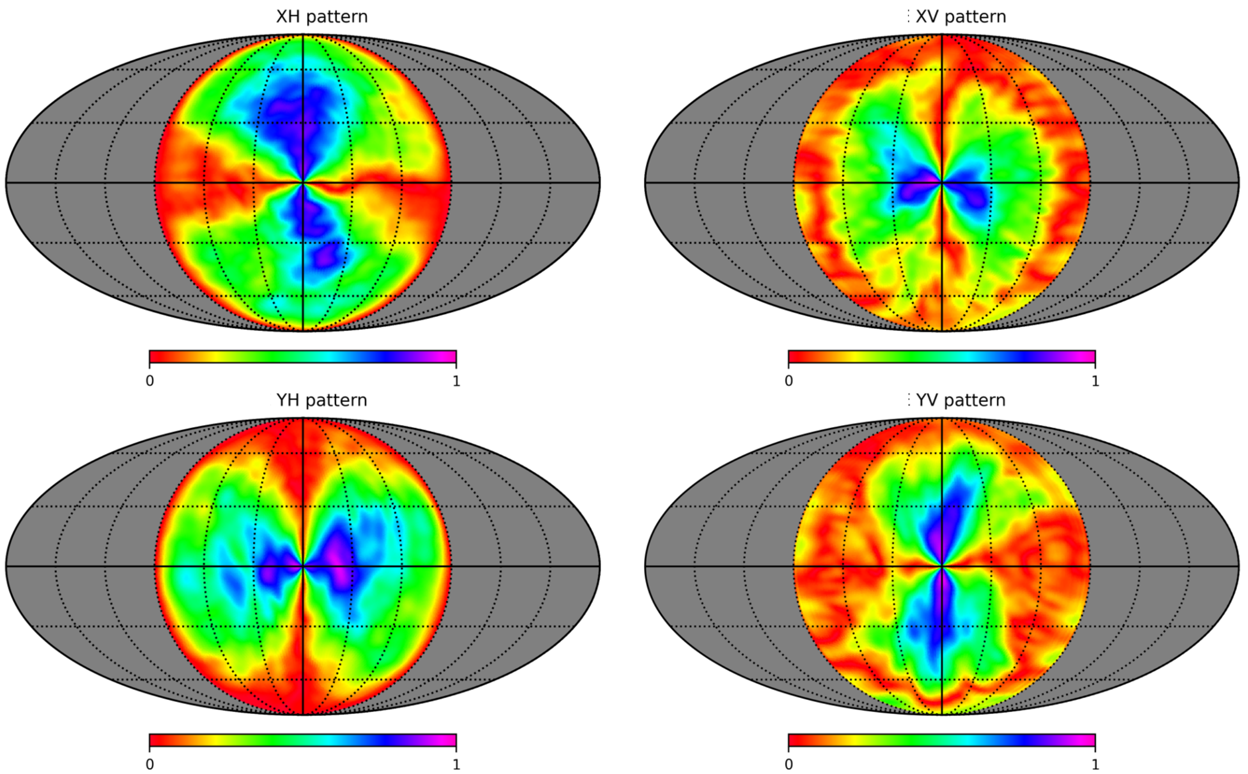

Figure 5 above shows the amplitudes of the embedded element patterns for one of the antennas in AAVS2. The images are in sky projection with North upwards, East to the left and zenith at the centre.

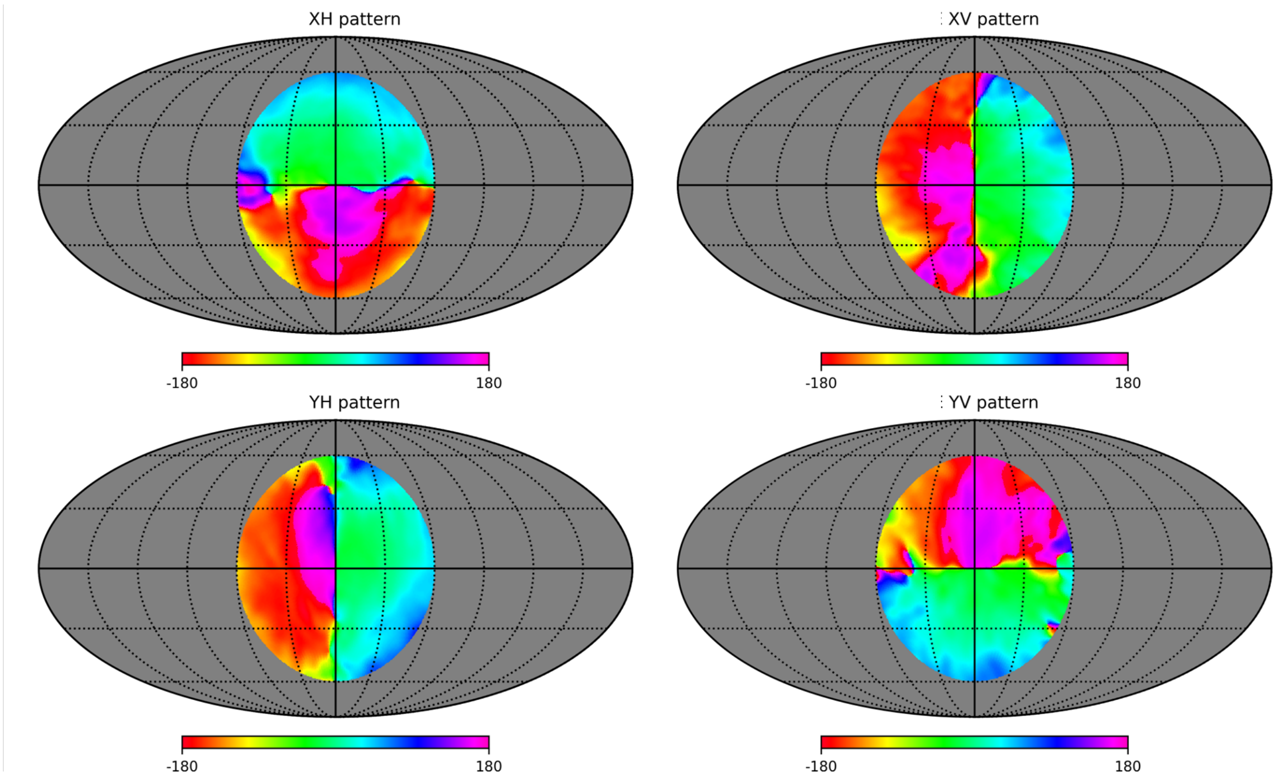

Figure 6 above shows the phase of the embedded element patterns for the same antenna, limited to elevations above 30 degrees.

In any sky direction and in the *H-V* frame towards that sky direction, the transformation of a Stokes visibility vector $[I'_v, Q'_v, U'_v, V'_v]^T$ to a coherency vector $[R_{HH}, R_{HV}, R_{VH}, R_{VV}]^T$ is described by the matrix operation:

$$\begin{bmatrix} R_{HH} \\ R_{HV} \\ R_{VH} \\ R_{VV} \end{bmatrix} = \begin{bmatrix} 1 & 1 & 0 & 0 \\ 0 & 0 & 1 & j \\ 0 & 0 & 1 & -j \\ 1 & -1 & 0 & 0 \end{bmatrix} \begin{bmatrix} I'_v \\ Q'_v \\ U'_v \\ V'_v \end{bmatrix}.$$

The Stokes intensities in any sky direction are, by convention, defined in a (χ, ψ) reference plane tangent to the celestial sphere that has χ axis locally towards North and ψ axis towards East. The right-handed coordinate system (χ, ψ, ω) at that location on the celestial sphere would have the positive of the third axis ω towards the observer. This is the cartesian referential defined by the International Astronomical Union [IAU, 1974, Transactions of the IAU Vol. 15B (1973) 166].

Towards any sky direction or position on the celestial sphere, the parallactic angle q is the position angle of zenith. This position angle at any position on the celestial sphere is, by definition, measured counterclockwise from North towards East, which is the angle measured counterclockwise from χ towards ψ. The vertical *V* axis of the (H, V) frame is towards zenith; therefore, rotation of the (χ, ψ) axes to (H, V) is a clockwise rotation through angle $(q - \pi/2)$ when viewed along the direction of propagation.

Imaging Method A

Computationally, the simplest implementation of rotation between the above IAU convention and the (H, V) frame is in the celestial sphere, where the 4-vector of Stokes intensities may be rotated; this is reasonable for snapshot imaging and for compact arrays where the parallactic angle for a sky pixel is the same as seen from all antennas. Thus for snapshot visibilities of AAVS2, we may adopt the measurement equation:

$$\begin{bmatrix} R_{XX} \\ R_{XY} \\ R_{YX} \\ R_{YY} \end{bmatrix} = \left(\begin{bmatrix} B_{1X\phi} B_{1X\theta} \\ B_{1Y\phi} B_{1Y\theta} \end{bmatrix} \otimes \begin{bmatrix} B^*_{2X\phi} B^*_{2X\theta} \\ B^*_{2Y\phi} B^*_{2Y\theta} \end{bmatrix} \right) \begin{bmatrix} 1 & 1 & 0 & 0 \\ 0 & 0 & 1 & j \\ 0 & 0 & 1 & -j \\ 1 & -1 & 0 & 0 \end{bmatrix} \begin{bmatrix} I'_v \\ Q'_v \\ U'_v \\ V'_v \end{bmatrix}.$$

In the custom Python script, the matrix for the transformation from $[I'_v, Q'_v, U'_v, V'_v]^T$ to $[R_{XX}, R_{XY}, R_{YX}, R_{YY}]^T$ is computed for each baseline and for each sky direction, using the embedded beam patterns for the pair of antennas forming the baseline. The calibrated coherency vector $[R_{XX}, R_{XY}, R_{YX}, R_{YY}]^T$ for each baseline is then matrix multiplied by the matrix inverse of this transformation matrix, to give the Stokes visibility vector $[I'_v, Q'_v, U'_v, V'_v]^T$ for that baseline, in the (H, V) frame for that sky direction.

At each timestamp, the Stokes visibilities $[I'_\nu, Q'_\nu, U'_\nu, V'_\nu]^T$ in (u, v, w) visibility domain are then 3D Fourier transformed to the celestial sphere, using the Fourier transform kernel

$$e^{-2\pi(ul+vm+wn)}.$$

The Fourier transformation yields Stokes intensity vectors $[I', Q', U', V']^T$ at (l, m, n) coordinates of sky pixels.

The minus sign in the exponent is chosen to be consistent with the convention in the computation of coherency vectors in the AAVS2 correlator (at least for the 21/22 April 2020 dataset). As mentioned above, for this adopted sign convention, the complex EM beam models provided by the EM simulations group need to be conjugated and then used as the terms $B_{X\phi}$, $B_{X\theta}$, $B_{Y\phi}$ and $B_{Y\theta}$ in the Jones matrices for the transformation.

In each sky direction, the Stokes intensity vector $[I', Q', U', V']^T$ is summed over all baselines and finally a direction-dependent rotation

$$\begin{bmatrix} I \\ Q \\ U \\ V \end{bmatrix} = \begin{bmatrix} 1 & 0 & 0 & 0 \\ 0 & cos(2q-\pi) & -sin(2q-\pi) & 0 \\ 0 & sin(2q-\pi) & cos(2q-\pi) & 0 \\ 0 & 0 & 0 & 1 \end{bmatrix} \begin{bmatrix} I' \\ Q' \\ U' \\ V' \end{bmatrix}$$

is made to get Stokes intensities $[I, Q, U, V]^T$ at all sky pixels in the (χ, ψ) frame. This yields Stokes intensities in the cartesian referential defined by the IAU.

Imaging Method B

In Earth-rotation synthesis imaging, parallactic angles of sky pixels change over time. Therefore, as a first step, parallactic angles of sky pixels at the visibility timestamp are used to rotate Stokes coherency vectors in individual baselines from (H, V) frame to IAU (χ, ψ) frame. Subsequently, all of the visibilities are Fourier transformed to celestial sphere. Of course, this assumes that the array is compact and the parallactic angle for a sky pixel is the same as seen from all antennas, which is a reasonable assumption for AAVS2.

$[I'_\nu, Q'_\nu, U'_\nu, V'_\nu]^T$ is the Stokes visibility vector in the (H, V) frame. If we denote the corresponding Stokes visibility vector in the (χ, ψ) frame to be $[I_\nu, Q_\nu, U_\nu, V_\nu]^T$, then

$$\begin{bmatrix} I'_\nu \\ Q'_\nu \\ U'_\nu \\ V'_\nu \end{bmatrix} = \begin{bmatrix} 1 & 0 & 0 & 0 \\ 0 & cos(2q-\pi) & sin(2q-\pi) & 0 \\ 0 & -sin(2q-\pi) & cos(2q-\pi) & 0 \\ 0 & 0 & 0 & 1 \end{bmatrix} \begin{bmatrix} I_\nu \\ Q_\nu \\ U_\nu \\ V_\nu \end{bmatrix}.$$

Putting it all together, the transformation from Stokes visibilities in IAU frame to coherency vector in antenna coordinates is

$$\begin{bmatrix} R_{XX} \\ R_{XY} \\ R_{YX} \\ R_{YY} \end{bmatrix} = \left(\begin{bmatrix} B_{1X\phi} B_{1X\theta} \\ B_{1Y\phi} B_{1Y\theta} \end{bmatrix} \otimes \begin{bmatrix} B^*_{2X\phi} B^*_{2X\theta} \\ B^*_{2Y\phi} B^*_{2Y\theta} \end{bmatrix} \right) \begin{bmatrix} 1 & 1 & 0 & 0 \\ 0 & 0 & 1 & j \\ 0 & 0 & 1 & -j \\ 1 & -1 & 0 & 0 \end{bmatrix} \begin{bmatrix} 1 & 0 & 0 & 0 \\ 0 & cos(2q-\pi) & sin(2q-\pi) & 0 \\ 0 & -sin(2q-\pi) & cos(2q-\pi) & 0 \\ 0 & 0 & 0 & 1 \end{bmatrix} \begin{bmatrix} I_v \\ Q_v \\ U_v \\ V_v \end{bmatrix}.$$

The matrices for field rotation and conversion from Stokes coherency vector to the coherency vector $[R_{HH}, R_{HV}, R_{VH}, R_{VV}]^T$ may be combined:

$$\begin{bmatrix} R_{XX} \\ R_{XY} \\ R_{YX} \\ R_{YY} \end{bmatrix} = \left(\begin{bmatrix} B_{1X\phi} B_{1X\theta} \\ B_{1Y\phi} B_{1Y\theta} \end{bmatrix} \otimes \begin{bmatrix} B^*_{2X\phi} B^*_{2X\theta} \\ B^*_{2Y\phi} B^*_{2Y\theta} \end{bmatrix} \right) \begin{bmatrix} 1 & cos(2q-\pi) & sin(2q-\pi) & 0 \\ 0 & -sin(2q-\pi) & cos(2q-\pi) & j \\ 0 & -sin(2q-\pi) & cos(2q-\pi) & -j \\ 1 & -cos(2q-\pi) & -sin(2q-\pi) & 0 \end{bmatrix} \begin{bmatrix} I_v \\ Q_v \\ U_v \\ V_v \end{bmatrix}.$$

In the custom Python 3 script, the matrix for the transformation from $[I_v, Q_v, U_v, V_v]^T$ to $[R_{XX}, R_{XY}, R_{YX}, R_{YY}]^T$ is computed for each baseline and for each sky direction, using the embedded beam patterns for the pair of antennas forming the baseline. The calibrated coherency vector $[R_{XX}, R_{XY}, R_{YX}, R_{YY}]^T$ for each baseline is then matrix multiplied by the matrix inverse of this transformation matrix, to give the Stokes visibility vector $[I_v, Q_v, U_v, V_v]^T$ for that baseline, in the (χ, ψ) frame for that sky direction.

Finally, the Stokes visibilities are Fourier transformed and accumulated in the celestial healpix sky pixels using the Fourier transform kernel:

$$e^{-2\pi(ul+vm+wn)}.$$

The Fourier transformation now directly yields Stokes intensity vectors $[I, Q, U, V]^T$ in IAU frame.

This method is the implementation in MIRIAD (see https://www.atnf.csiro.au/computing/software/miriad/userguide/node74.html) for rotation of feeds with respect to sky over the synthesis observation.

Imaging Method C

A third and more exact formulation is to treat the field rotation for the i-th antenna as a direction dependent Jones matrix:

$$\begin{bmatrix} E_{iH} \\ E_{iV} \end{bmatrix} = \begin{bmatrix} sin(q_i) & -cos(q_i) \\ cos(q_i) & sin(q_i) \end{bmatrix} \begin{bmatrix} E_{i\chi} \\ E_{i\psi} \end{bmatrix}$$

that transforms the incident EM wave components in IAU (χ, ψ) frame to EM wave components in (H, V) frame.

Combining the Jones matrices for beam patterns with the above Jones matrix for field rotation:

$$\begin{bmatrix} E_{iX} \\ E_{iY} \end{bmatrix} = \begin{bmatrix} B_{iX\phi} B_{iX\theta} \\ B_{iY\phi} B_{iY\theta} \end{bmatrix} \begin{bmatrix} sin(q_i) & -cos(q_i) \\ cos(q_i) & sin(q_i) \end{bmatrix} \begin{bmatrix} E_{i\chi} \\ E_{i\psi} \end{bmatrix}$$

The coherency vector for any baseline from antenna 1 to antenna 2 may be written as

$$\begin{bmatrix} R_{XX} \\ R_{XY} \\ R_{YX} \\ R_{YY} \end{bmatrix} = \left\{ \begin{bmatrix} B_{1X\phi} B_{1X\theta} \\ B_{1Y\phi} B_{1Y\theta} \end{bmatrix} \begin{bmatrix} sin(q_1) & -cos(q_1) \\ cos(q_1) & sin(q_1) \end{bmatrix} \begin{bmatrix} E_{1\chi} \\ E_{1\psi} \end{bmatrix} \right\} \otimes \left\{ \begin{bmatrix} B_{2X\phi} B_{2X\theta} \\ B_{2Y\phi} B_{2Y\theta} \end{bmatrix} \begin{bmatrix} sin(q_2) & -cos(q_2) \\ cos(q_2) & sin(q_2) \end{bmatrix} \begin{bmatrix} E_{2\chi} \\ E_{2\psi} \end{bmatrix} \right\}$$

$$= \left\{ \begin{bmatrix} B_{1X\phi} B_{1X\theta} \\ B_{1Y\phi} B_{1Y\theta} \end{bmatrix} \otimes \begin{bmatrix} B_{2X\phi} B_{2X\theta} \\ B_{2Y\phi} B_{2Y\theta} \end{bmatrix} \right\} \left\{ \begin{bmatrix} sin(q_1) & -cos(q_1) \\ cos(q_1) & sin(q_1) \end{bmatrix} \otimes \begin{bmatrix} sin(q_2) & -cos(q_2) \\ cos(q_2) & sin(q_2) \end{bmatrix} \right\} \begin{bmatrix} R_{\chi\chi} \\ R_{\chi\psi} \\ R_{\psi\chi} \\ R_{\psi\psi} \end{bmatrix}$$

$$= \left\{ \begin{bmatrix} B_{1X\phi} B_{1X\theta} \\ B_{1Y\phi} B_{1Y\theta} \end{bmatrix} \otimes \begin{bmatrix} B_{2X\phi} B_{2X\theta} \\ B_{2Y\phi} B_{2Y\theta} \end{bmatrix} \right\} \left\{ \begin{bmatrix} sin(q_1) & -cos(q_1) \\ cos(q_1) & sin(q_1) \end{bmatrix} \otimes \begin{bmatrix} sin(q_2) & -cos(q_2) \\ cos(q_2) & sin(q_2) \end{bmatrix} \right\} \begin{bmatrix} 1 & 1 & 0 & 0 \\ 0 & 0 & 1 & j \\ 0 & 0 & 1 & -j \\ 1 & -1 & 0 & 0 \end{bmatrix} \begin{bmatrix} I_v \\ Q_v \\ U_v \\ V_v \end{bmatrix}$$

where q_1 and q_2 are parallactic angles of the sky pixel as viewed from antennas 1 and 2.

In the custom Python 3 script, the matrix for the transformation from $[I_v, Q_v, U_v, V_v]^T$ to $[R_{XX}, R_{XY}, R_{YX}, R_{YY}]^T$ is computed for each baseline and for each sky direction, using the embedded beam patterns for the pair of antennas forming the baseline. The calibrated coherency vector $[R_{XX}, R_{XY}, R_{YX}, R_{YY}]^T$ for each baseline is then matrix multiplied by the matrix inverse of this transformation matrix, to give the Stokes visibility vector $[I_v, Q_v, U_v, V_v]^T$ for that baseline, in the IAU (χ, ψ) frame for that sky direction.

Finally, the Stokes visibilities are Fourier transformed and accumulated in the celestial healpix sky pixels using the Fourier transform kernel:

$$e^{-2\pi(ul+vm+wn)}.$$

The Fourier transformation directly yields Stokes intensity vectors $[I, Q, U, V]^T$ in IAU frame.

Limiting errors at low elevations

All of the above measurement equations include a position-dependent correction for the dissimilar EEP beam patterns of the antennas in the station. The correction is made by effectively dividing the measured coherency vector by the beam response; therefore, in sky directions where the product of the complex beam patterns for a baseline is erroneously small, the baseline contributes a large spurious intensity. In the Fourier transform from baseline visibilities to sky intensities, the summation at any sky pixel might be dominated by anomalous contributions from a few such baselines, and avoidance of this imaging error requires an algorithm for rejecting such erroneous contributions.

The imaging process multiplies the coherency vector $[R_{XX}, R_{XY}, R_{YX}, R_{YY}]^T$ by the inverse of the matrix:

$$M = \left(\begin{bmatrix} B_{1X\phi} B_{1X\theta} \\ B_{1Y\phi} B_{1Y\theta} \end{bmatrix} \otimes \begin{bmatrix} B^*_{2X\phi} B^*_{2X\theta} \\ B^*_{2Y\phi} B^*_{2Y\theta} \end{bmatrix} \right) \begin{bmatrix} 1 & 1 & 0 & 0 \\ 0 & 0 & 1 & j \\ 0 & 0 & 1 & -j \\ 1 & -1 & 0 & 0 \end{bmatrix}$$

For each baseline and sky pixel, the inverse of matrix M is computed, the absolute values of the complex numbers in M^{-1} is evaluated, and the maximum of these is compared to a threshold. For the voltage beam patterns of AAVS2 station at 110 MHz, I have adopted a threshold that corresponds to rejecting pixel-baseline combinations where the beam response is less than 20%. The adopted algorithm requires careful revision and fine tuning if useful polarisation beam forming is to be done at low elevations below about 30 degrees.

I have prepared Python 3 scripts that implement all three methods — A, B & C — described above; unsurprisingly, for intra-station correlations of AAVS2, all three methods give identical results.

Example Stokes Images

I show below (in the following pages Figs. 7 & 8; upper panels) snapshot images in Stokes I, Q, U and V made at representative times when the Sun was at maximum elevation and when the Galactic Centre was close to zenith at the MRO site.

The Stokes images presented here have not been deconvolved. Image intensities are in units of kelvin brightness. The images are “naturally” weighted, with all baselines given equal weights. The healpix images were synthesised with NSIDE = 32, corresponding to pixels 109.9 arcmin in size and providing a sampling of the sky of about two points per synthesised beam FWHM. The healpix images were then interpolated to a finer grid with NSIDE=128 for display.

An example of the primary beam is shown below in Fig. 9 corresponding to the image made at UT 20 hr. The primary beam response is at lowest 0.233 at elevation 30 degrees.

Figure 9 shows the primary beam for the image towards Galactic Centre, in Galactic coordinates, limited to elevations above 30 degrees. The image is in sky projection with North upwards, East to the left and zenith at the

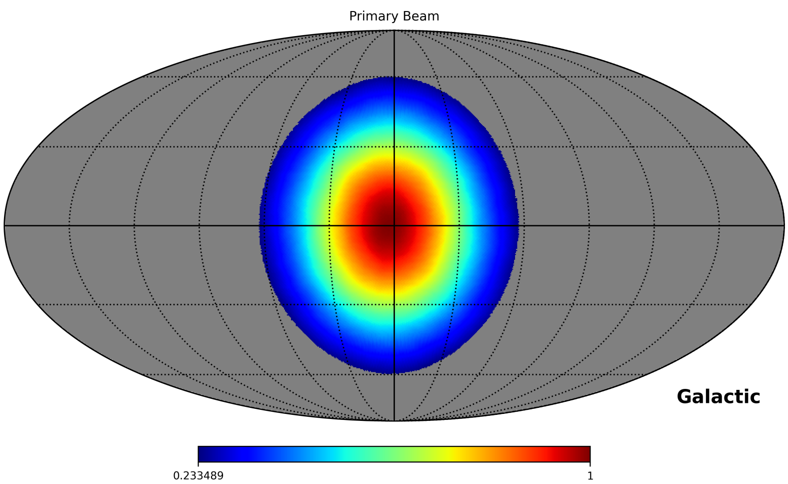

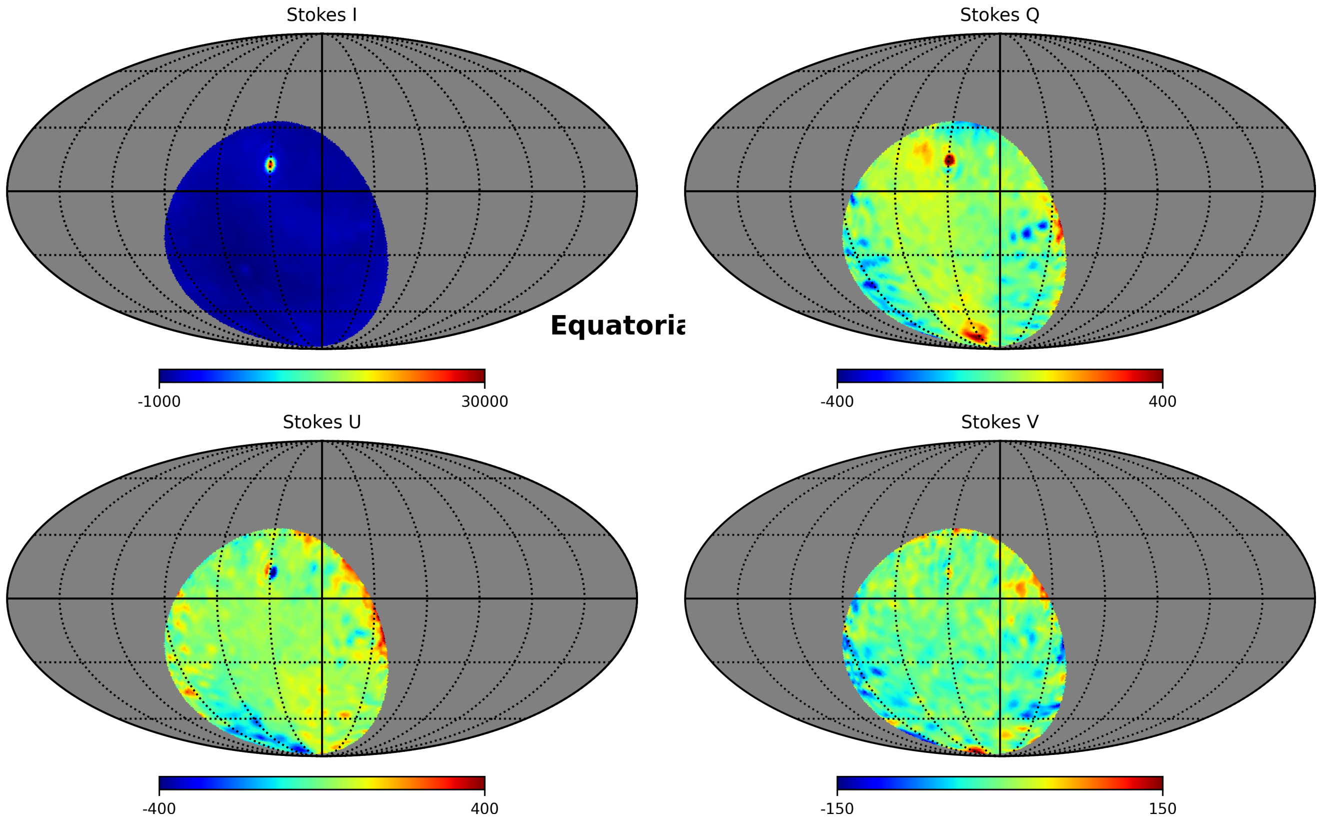

Figure 7:
Panels above show Stokes images made using calibrated measured visibilities at 04 UT close to the time when the Sun crossed the celestial meridian. Images are limited to elevation angles above 30 degrees. Display of all-sky healpix maps are in kevin brightness temperature and in Mollweide projection in equatorial coordinates. The images are tapered by the average EEP power pattern. Panels below show corresponding Stokes images made using model visibilities predicted from Global Sky Model plus Sun, both unpolarised. Predictions and imaging use EEP patterns.

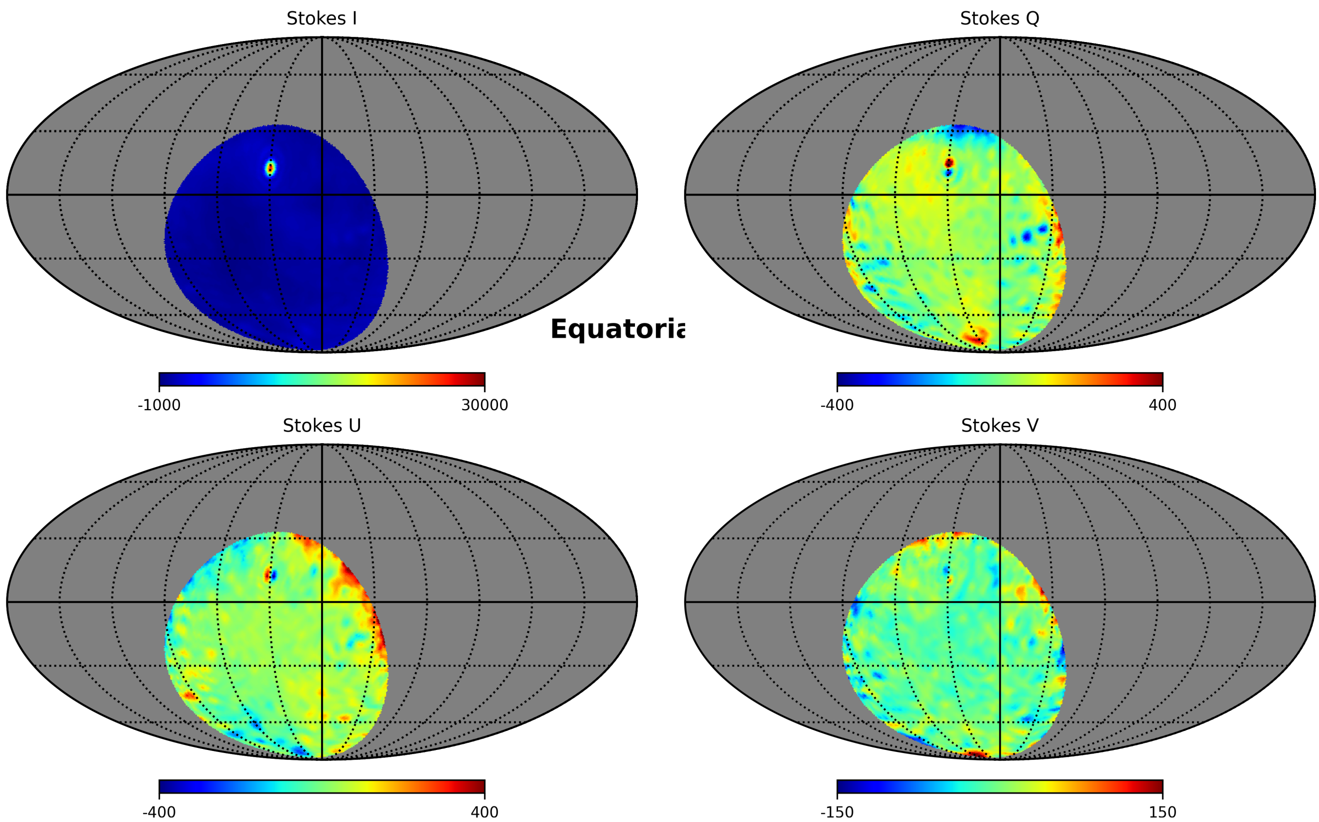

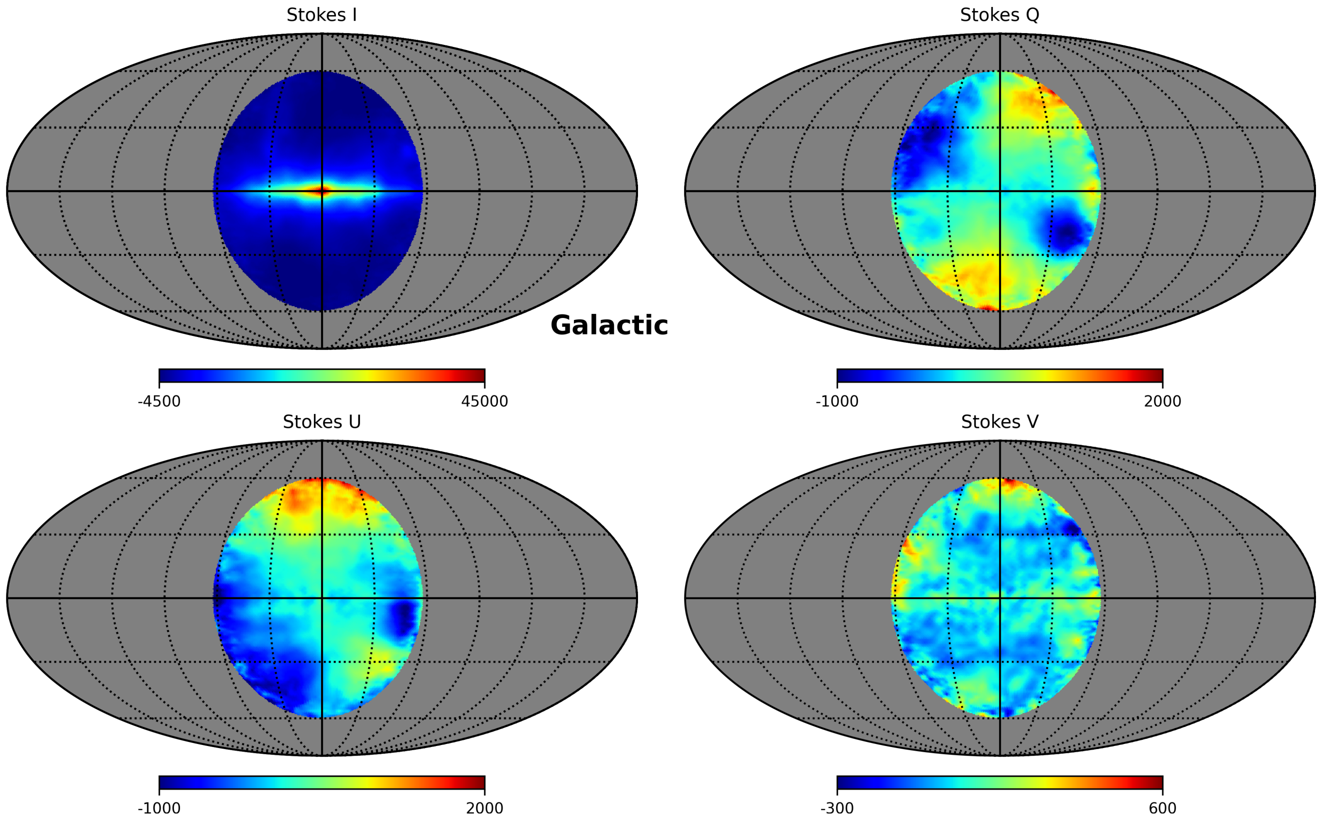

Figure 8:
Panels above show Stokes images made using calibrated measured visibilities at 20 UT at about the time when the Galactic centre was close to zenith at MRO. Images are limited to elevation angles above 30 degrees. Display of all-sky healpix maps are in Mollweide projection in Galactic coordinates. The images are in kelvin scale of brightness temperature and tapered by the average EEP power pattern.
Panels below show Stokes images made using model visibilities predicted from Global Sky Model plus Sun, both unpolarised. Predictions and imaging use EEP patterns.

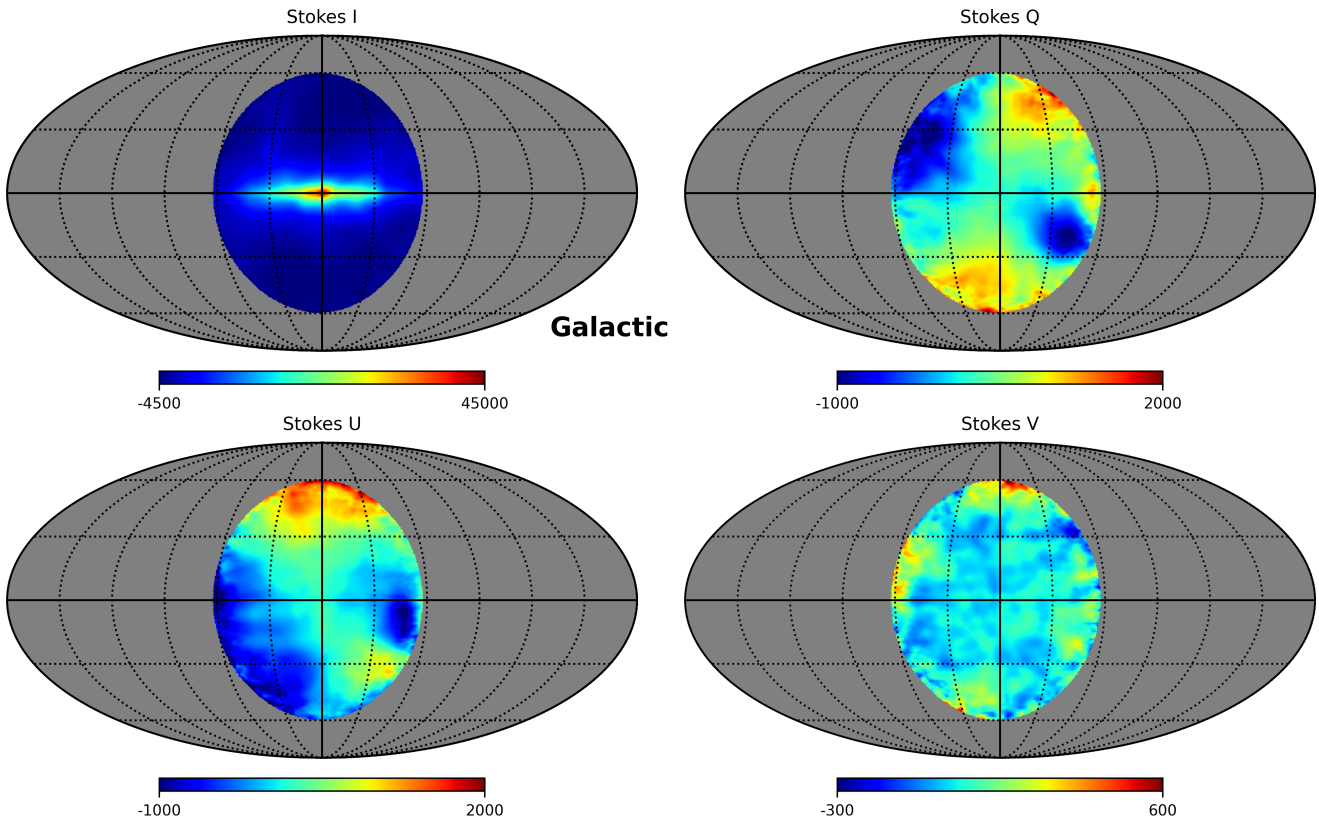

Polarisation purity

The Stokes Images in Q, U and V shown in the upper panels of Figs. 7 & 8, made from calibrated visibility products, have structure all over the sky. The structures; in particular that in Stokes V images, are almost certainly spurious.

In an attempt at understanding the cause of these structures, I have predicted visibilities in XX, XY, YX and YY products using a model sky that is the Global Sky Model [Zheng et al. 2016] plus the Sun as a pixel with brightness corresponding to the flux density in Benz [2009 Astronomy & Astrophysics, Vol. 4B, p.103]. EEP patterns were used for the prediction. These model visibilities were then imaged to the healpix sky grid again using EEP patterns as discussed above. The Stokes images constructed from model visibilities are shown in the lower panels in Figs. 7 & 8.

It is remarkable that there is striking similarity in the Stokes Q, U and V polarisation distributions in images made using model visibilities and those made using the calibrated measurements from AAVS2. Thus, for the polarisation calibration method adopted, including that for the XY phase, the dominant limiting factor to polarisation purity is not station calibration. My inference is that the dominant limitation to polarisation purity in the Stokes imaging/beamforming with AAVS2 station is currently the accuracy of the EEP beam patterns, on average. I expand on this below.

If we have an unpolarised source in a particular sky position, it will result in XX, XY, YX, YY correlation products depending on the voltage beam patterns of the X and Y feeds of the antennas forming the baseline. Let us assume that these products are precisely calibrated for the X and Y receiver complex gains, including XY phase.

(a) If we then image these visibilities back to sky using accurate EEP beam patterns to correct for the antenna responses, then we expect to get an unpolarised pixel at the source location. Since the source is unpolarised, we would expect that if the EEP patterns are accurate, then Stokes Q, U and V ought to be zero across the sky whereas Stokes I image would be the point spread function (synthetic beam pattern) centred on the location of the unpolarised source.
(b) However, if the EEP patterns are inexact, there would be residual Stokes Q, U and V at the source location in the image. Additionally, the beam patterns do not exactly cancel Stokes Q, U and V over the sky and hence we get a residual polarisation over the whole sky. This limitation is not due to the synthesised beam sidelobes of the station array configuration but due to the inaccuracy in EEP voltage patterns. This spillover of Stokes I into polarisation could be viewed as a polarisation leakage arising from inaccurate beam model.

Examining sky images made at 04 UT, when the Sun was at maximum elevation, the standard deviation in Stokes Q and U image pixels is 47 K and that in Stokes V image is 16 K, in pixels in quadrants excluding the location of the Sun. These are 0.2% and 0.06% of the Stokes I intensity of the Sun, which is 28,059 K as observed attenuated by the beam pattern. As seen in the comparison images displayed in lower panels of Figs. 7 & 8, the Stokes Q, U and V images made using mock visibilities have peak-to-peak polarisation leakage similar to that in the images made from measurement data (upper panels); the standard deviations in Stokes Q & U images made using mock visibilities are at 0.15% and that in Stokes V is 0.05%, similar to that of the measurement data.

The above polarisation leakage is when a single source — the Sun — dominates the sky. As a confirmation, I have adopted a model sky with just a single unresolved source, computed visibility products using EEPs, and imaged the sky again using EEPs. The simulation shows that any Stokes I source on the sky results in polarisation leakage over the entire sky with standard deviation between 0.06—0.15% in Stokes Q & U and at a level 0.02—0.05% in Stokes V, depending on the source location. These are of similar fractional magnitude compared to the polarisation leakage in AAVS2 images containing the Sun.

In images made when the Galactic centre is close to zenith and the brightest parts of the Galaxy are in the beam of the station antennas, the sky brightness in Stokes I is at maximum and hence the integrated polarisation leakage from all of the Galaxy in the field of view is at its worst. At this time, the polarisation images have standard deviations of 370 K in Stokes Q & U and 55 K in Stokes V. These are less than 1% of the Stokes I peak of 44,670 K; however, they are a substantial fraction of the mean brightness of the sky at this frequency, which is 860 K.

Another characterisation of the polarisation leakage in the station beams may be done by examining Stokes Q, U and V brightness at the positions of bright sources — Sun, Galactic Centre — as they drift across the sky over a range of elevation/azimuth.

Shown below in Fig. 9 are traces of Stokes intensities and their ratios, in bright pixels. Pixels containing the Sun and pixels in the brightest parts of the Galactic plane are tracked, while they are observed at high elevations above 45 degrees. Images have been corrected for the attenuation due to the primary beam before extracting the pixel intensities.

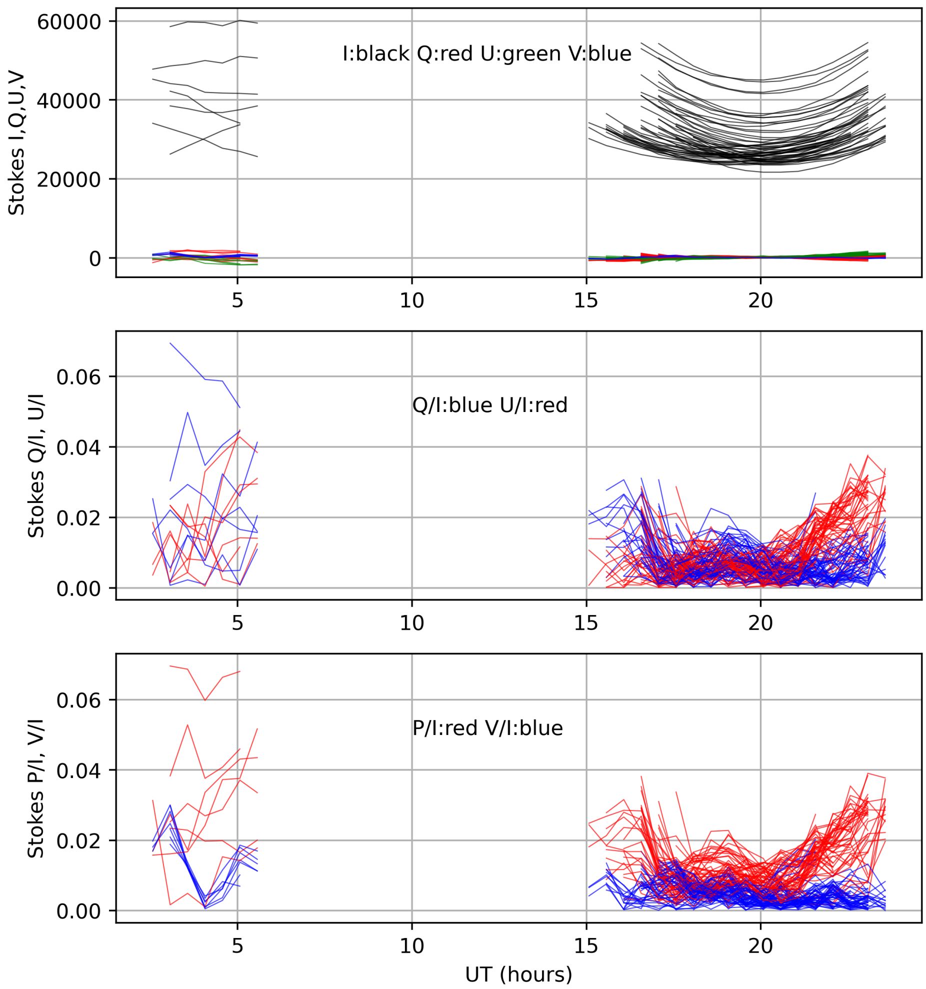

Figure 9: Stokes Intensities and their ratios versus time. Only pixels that are bright in Stokes I are included and their intensities tracked over time and while they are above elevation limit of 45 degrees. On the left, over the range UT 2—6 hrs, are traces of pixels containing the Sun; on the right and in the UT time range 15—24 hrs are pixels on the galactic plane.

In Fig. 10 is shown traces of Stokes intensity ratios, towards just the pixels containing peak brightness towards the Sun and Galactic Centre, while these pixels are above 30 degrees elevation angle.

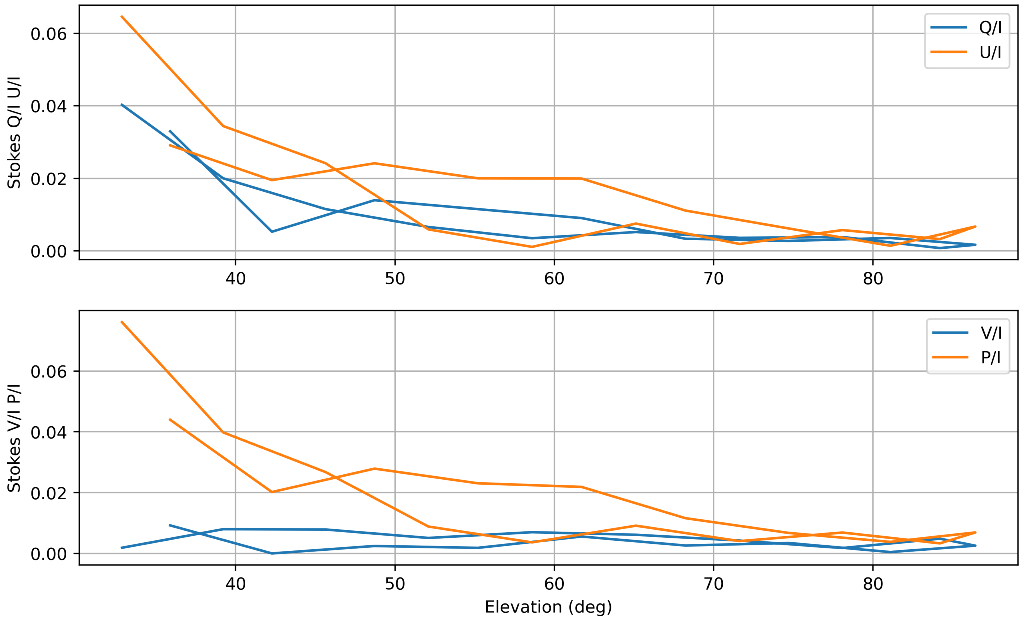

Figure 10: The polarisation in the brightest pixel towards Galactic centre is shown in panels above and polarisation towards the Sun is shown below, as the strong sources drift across the sky, across azimuth and elevation and across the antenna beam patterns. The upper panels show ratios of Stokes Q & U intensities to Stokes I, lower panels shows ratios of linear polarisation P and Stokes V to Stokes I: $\left(\sqrt{Q^2+U^2}\right)/I$ and V/I.

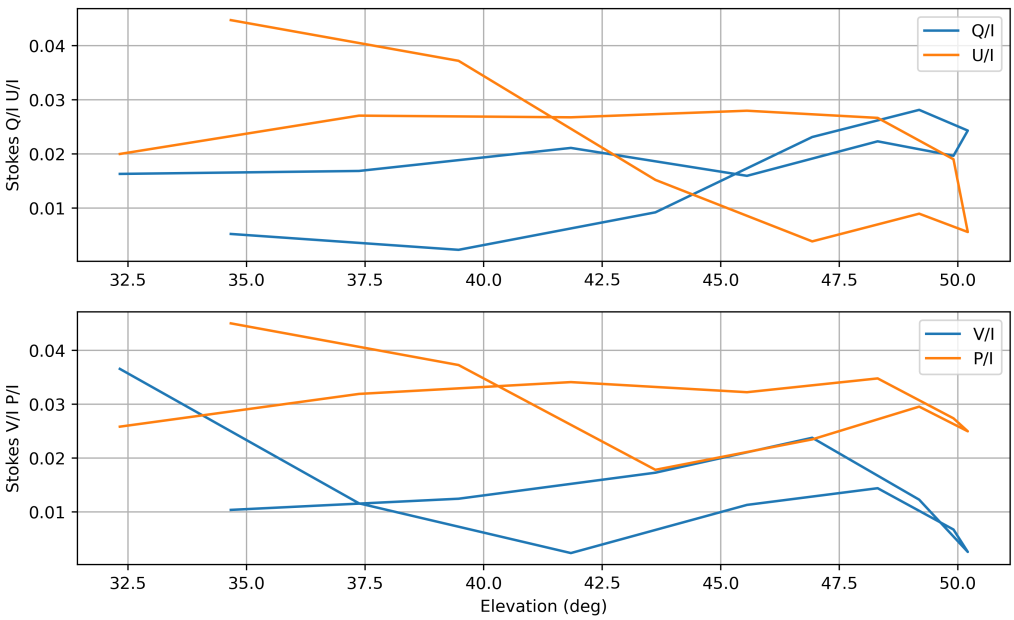

The Sun might be polarised; however, the bright parts of the Galaxy are expected to have small polarisation due to large Faraday depths. The imaging algorithm and accuracy in EEP patterns is seen to yield polarisation purity of better than 3% in Stokes Q and U and 1% in Stokes V, for elevations above 45 degrees.

It may be noted here that the polarisation leakage appears dominated by error in the average EEP pattern, with variations amongst antennas playing a relatively minor role. There appears to be a systematic error in the computation of EEPs, affecting all antennas in the station.

The basis for this proposition is that when the visibilities are imaged using the average EEP pattern for all antennas in the array (Figs. 3 & 4), the dominant structure in Stokes Q, U and V is same as that in Figs. 7 & 8. Stokes images made using average EEPs, at UT 04 hrs and 20 hrs, are shown in Fig. 11 for comparison with those in Figs. 7 & 8 that were constructed using EEPs.

A path to improving polarisation purity in station beams

If the dominant limitation to polarisation purity is in the average pattern, as a systematic error in all antennas of the array, the first step in improving polarisation purity might be in solving for a direction-dependent common-mode correction to the antenna EEP voltage patterns.

Since the number of independent sky pixels is much smaller than the number of independent visibility measurements; therefore, it may be possible to use a global sky model along with visibility measurements of all polarisation products to jointly solve for antenna X and Y complex gains, XY phase, and a common direction dependent correction to the EEPs of all antennas. This is potential work for the future, if improving the station beam polarisation purity beyond current limits is of value to SKA-LOW imaging.

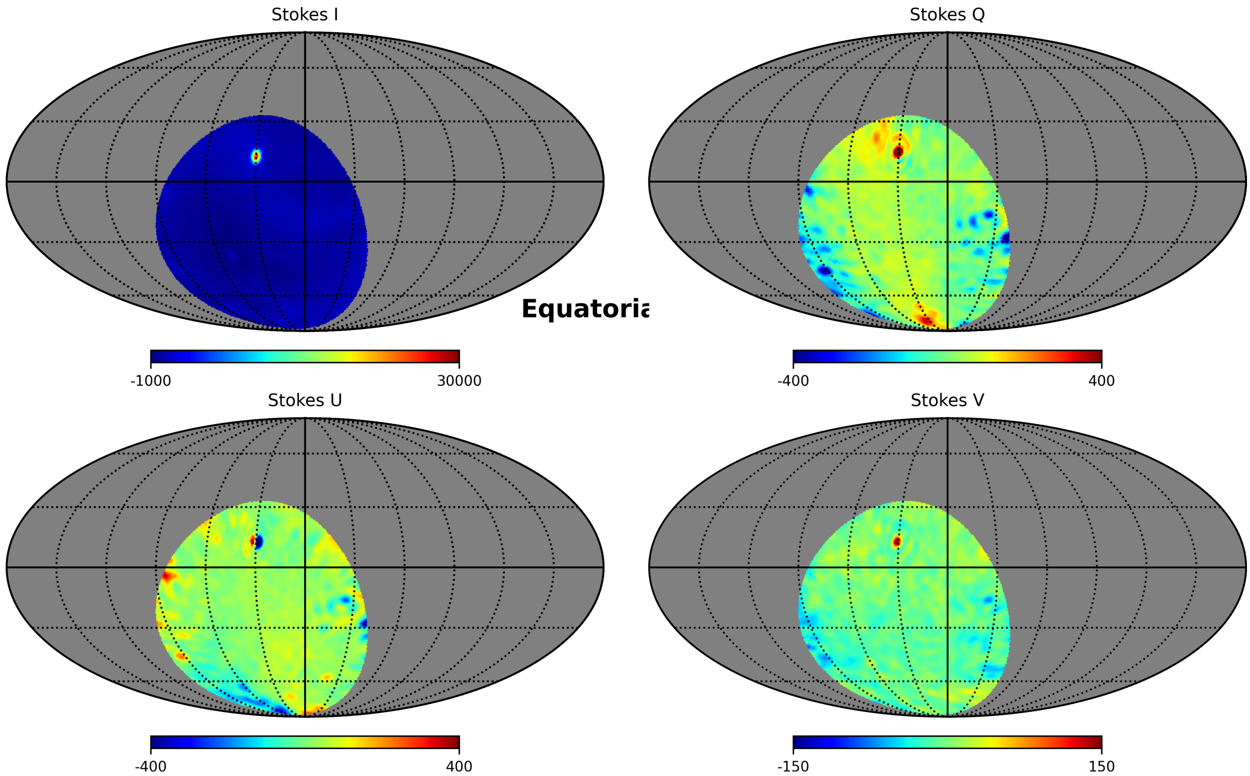

Figure 11: Stokes images made using the calibrated visibilities at UT 04 hrs (above, in equatorial coordinates) and UT 20 hrs (below, in galactic coordinates). These images were constructed using the average EEP patterns shown in Fig. 3 & 4, assuming identical patterns for all antennas in the station. Images are limited to elevation angles above 30 degrees. Display of all-sky healpix maps are in kevin brightness temperature and in Mollweide projection; images are tapered by the average EEP power pattern.